Journal of Molecular Structure 987 (2011) 25–33

Contents lists available at ScienceDirect

Journal of Molecular Structure

journal homepage: www.elsevier.com/locate/molstruc

Vibrational and crystal structure analysis of a phenylenedioxydiacetic acid derivative

Benjamin V. Cunning [a], Gregory A. Hope [a], Peter C. Healy [b], Christopher L. Brown [a,*]

[a] Queensland Micro- and Nanotechnology Centre, Griffith University, Brisbane, Qld, 4111, Australia
[b] School of Biomolecular and Physical Sciences, Griffith University, Brisbane, Qld, 4111, Australia

ARTICLE INFO

Article history:
Received 16 September 2010
Received in revised form 18 November 2010
Accepted 18 November 2010
Available online 29 November 2010

Keywords:
Vibrational spectroscopy
X-ray diffraction
Crystal packing forces and density functional theory calculations

ABSTRACT

Computationally derived data has successfully assisted the characterisation of the Raman and infrared vibrational spectra of the phenylenedioxydiacetic acid (PDA) derivative 2,2′-[(4-nitro-1,2-phenylene)bis(oxy)]diacetate (I) in the solid state. X-ray diffraction analysis of (I), which crystallised in the non-centrosymmetric achiral space group $Pca2_1$, revealed the computationally predicted minimum energy geometry differed to that observed in the solid state molecule due to significant inter-molecular bonding, this was also confirmed computationally. Importantly, large deviations between the wavenumber of predicted and experimental vibrational modes only occurred with functional groups that engaged in inter-molecular bonding. From a comparison of the energies of the calculated and X-ray structural data the crystal packing forces in the solid-state was estimated at ≈240 kJ/mol.

1. Introduction

Crystal packing forces form an integral part in the three dimensional arrangement of both biological and non-biological macromolecules. Understanding the nature of these interactions has numerous applications in drug design, crystal engineering, and understanding biological processes.

Computational chemistry packages have made the prediction of molecular properties from small organic molecules to large proteins a relatively straightforward task. The vast majority of these packages, however, perform optimisations and calculations on a single molecule in the gaseous phase and this may not be representative of bulk phase molecules in the solid state. Whilst these calculations may fortuitously afford acceptable results for simple systems; the subtle inter-molecular non-bonded interactions that can often dominate in larger solid systems often result in the poor prediction of their molecular properties.

Ongoing studies into the coordination chemistry of analogues of 1,2-phenylenedioxydiacetic acid (PDA) has resulted in the synthesis of dimethyl 2,2′-[(4-nitro-1,2-phenylene)bis(oxy)]diacetate (I) (Fig. 1). This class of molecules comprise tetradentate ligands possessing two ether oxygen atoms and two carboxylate oxygen atoms and are capable of forming coordination complexes with moderately hard metals, including the uranyl ion $\left(UO_2^{2+}\right)$ [1], lanthanides in the +3 oxidation state [2], bismuth in the +3 oxidation state [3], and various transition metals in the +2 oxidation state [4].

The flexible arms substituted on the 1 and 2 positions of the benzene ring, in addition to the nitro group located at the 4 position, provides potential for differences in inter-molecular interactions within the solid phase environment. This may result in substantially different molecular properties (such as vibrational mode frequencies and the minimum energy geometries) from those predicted by single molecule gas phase quantum chemical calculations.

2. Experimental

2.1. Materials

4-Nitrocatechol and methyl bromoacetate were obtained from Sigma–Aldrich (Australia). The solvents were of AR grade and obtained from Merck (Australia). Potassium carbonate was obtained from Chem-Supply (Australia). All materials were used without further purification.

2.2. Synthesis of (I)

4-Nitrocatechol (4.00 g, 25.8 mmol) was dissolved in dimethylformamide (100 mL) to which potassium carbonate (9.73 g, 70.4 mmol) was subsequently added forming a slurry. A solution of methyl bromoacetate (10.76 g 70.3 mmol) and dimethylformamide (10 mL) was added dropwise over a period of five minutes at room temperature. The reaction was then stirred at 80 °C under a drying tube ($CaCl_2$) for 12 h. The reaction slurry was filtered, and the retentate rinsed with acetone (3 × 50 mL portions). The

* Corresponding author. Tel.: +61 7 37357293; fax: +61 7 37357656.
E-mail address: c.l.brown@griffith.edu.au (C.L. Brown).

0022-2860/$ - see front matter © 2010 Elsevier B.V. All rights reserved.
doi:10.1016/j.molstruc.2010.11.055

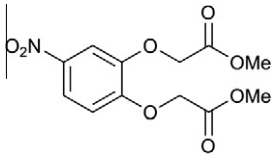

Fig. 1. A representative view of (I).

solvents from the combined organic phase were removed under reduced pressure and the residue partitioned between ethyl acetate and water (75 mL of each). The organic layer separated and subsequently washed twice with water (50 mL), and then dried using anhydrous sodium sulphate. The residue after solvent removal was recrystallised twice from pure ethanol yielding 4.32 g (14.4 mmol, 56%) of material (long needle-like crystals of up to 1 cm in length). Single crystals suitable for X-ray analysis were grown by slowly cooling a warm ethanol solution in an insulated vessel followed by slow evaporation of the ethanol solvent.

^{1}H NMR (400 MHz, $CDCl_3$) δ 7.92 (dd, J = 9.0, 2.6 Hz, 2H), 7.74 (d, J = 2.6 Hz, 2H), 6.88 (d, J = 9.0 Hz, 2H), 4.83 (s, 2H), 4.80 (s, 2H), 3.83 (s, 3H), 3.81 (s, 3H).
^{13}C NMR (100 MHz, $CDCl_3$) δ 168.48, 168.32, 153.20, 147.59, 142.40, 118.89, 113.23, 110.09, 66.37, 66.24, 52.66.
MS(ES+) calculated M + Na 322.05 *m/z*; found M + Na 321.83 *m/z*.

2.3. X-ray crystallography

A unique data set for (I) was measured on an Oxford-Diffraction GEMINI S Ultra CCD diffractometer at 200 ± 1 K (Mo–K_α radiation λ = 0.71069 Å) to 2θmax = 50°. The structure was solved by direct methods and refined by full matrix least squares refinement on F^2 after application of empirical absorption corrections. Anisotropic thermal parameters were refined for non-hydrogen atoms; (x, y, z, U_{iso})$_H$ were included and constrained at estimated values. Conventional residuals at convergence are quoted; statistical weights were employed. Computation used the teXsan [5] CrysAlis [6], SHELXL97 [7], ORTEP-3 [8] and PLATON [9] program and software systems. A full .cif deposition resides in both the supplementary data and the Cambridge Crystallographic Data Centre with CCDC number 791829. Copies of the data may be obtained free of charge from the Director, CCDC, 12 Union Road, Cambridge, CB2 1EZ. UK at the following address: http://www.ccdc.cam.ac.uk/cgi-bin/catreq.cgi.

Crystal Data for $C_{12}H_{13}NO_8$ M = 299.23, orthorhombic, space group $Pca2_1$, a = 11.5978(8), b = 14.7402(11), c = 7.7831(6) Å, U = 1330.5(2) Å^3, Z = 4, D_c = 1.49 g cm^{-3}, μ = 0.128 mm^{-1}, Crystal size: 0.33 × 0.15 × 0.14 mm. $T_{min/max}$ = 0.96, 0.98.

6153 Reflections collected, 1275 unique (R_{int} = 0.030), R = 0.025 [938 reflections with $I > 2\sigma(I)$], wRF^2 = 0.045 (all data). A thermal ellipsoid plot is shown in Fig. 2.

2.4. Vibrational spectroscopy

Raman spectra of (I) were collected on a Renishaw InVia spectrometer, excited using a 632.8 nm HeNe laser. The radiation was focused through a 50× Leica N Plan lens, and was measured at ~10 mW. The samples for Raman were prepared by focusing the radiation directly onto the crystalline material. The resultant spectrum is shown in Fig. 3.

IR spectroscopy was performed using a Thermo Nicolet Nexus FT-IR spectrometer equipped with EverGlo IR source optics at a

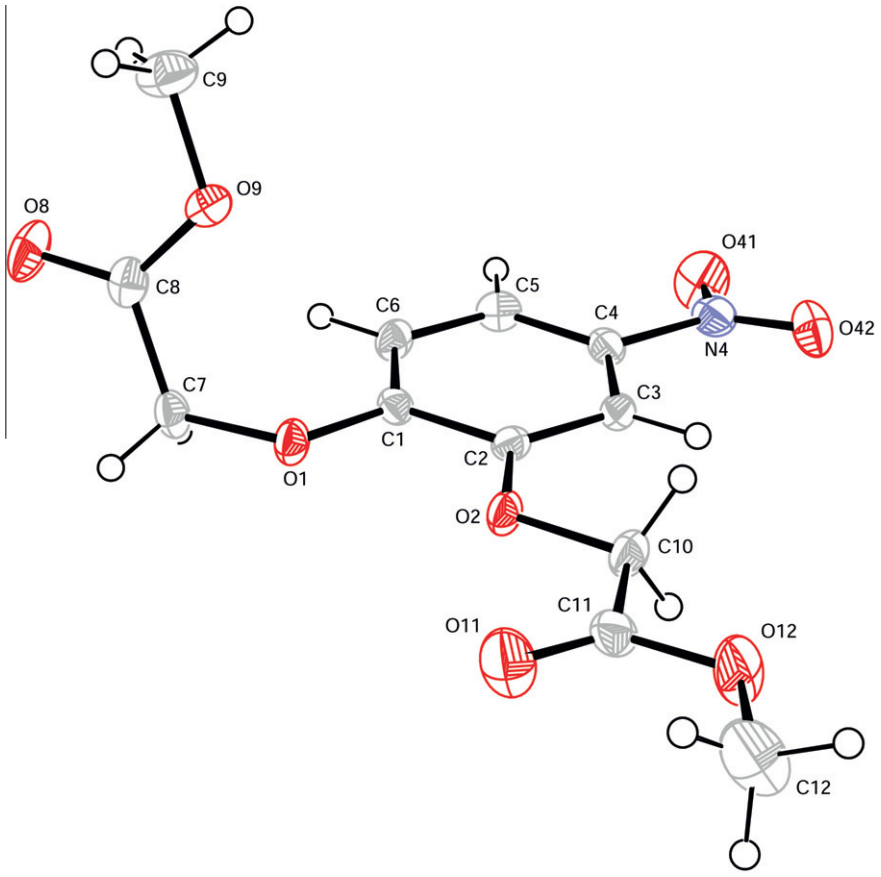

Fig. 2. A thermal ellipsoid plot of (I).

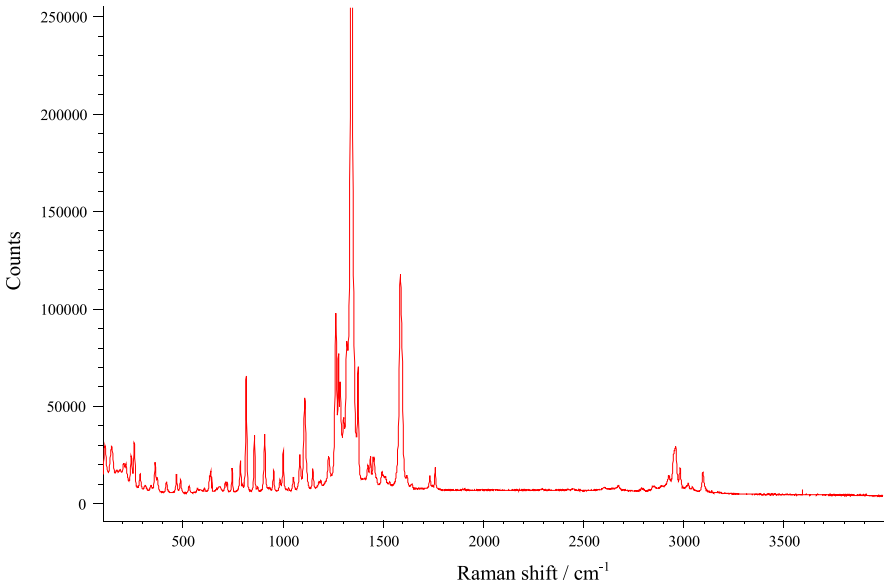

Fig. 3. The Raman spectrum of (I).

resolution of 2 cm^{-1}. The samples for infrared were dispersed within KBr forming a thin disc. The spectrum is shown in Fig. 4.

2.5. Computational studies

Single point calculations, geometry optimisation and vibrational calculations were performed using the hybrid functional B3LYP as implemented in Gaussian 03 [10]. Interaction energy calculations were performed at the MP2 level, with basis set superposition error taken into account *via* counterpoise correction. The basis set used was 6-31G augmented with diffuse functions given by the parameter "++" in the Gaussian 03 command file. A frequency factor of 0.96 was applied to all frequencies [11]. Potential energy distribution (PED) analysis was performed with the aid of the VEDA4 package [12]. The geometric coordinates of the minimum energy geometry structure are available in the supplementary data.

3. Results and discussion

The vibrational assignments subsequently discussed are summarised below in Table 1.

3.1. Vibrations attributed to C–H bonds

A tri-substituted benzene ring gives rise to three aromatic C–H stretches, which were calculated to occur at 3145, 3136 and 3108 cm^{-1}. Analysis of the infrared spectrum of (I) locates these bands at 3096 and 3042 and 3021 cm^{-1}. Analysis of the Raman

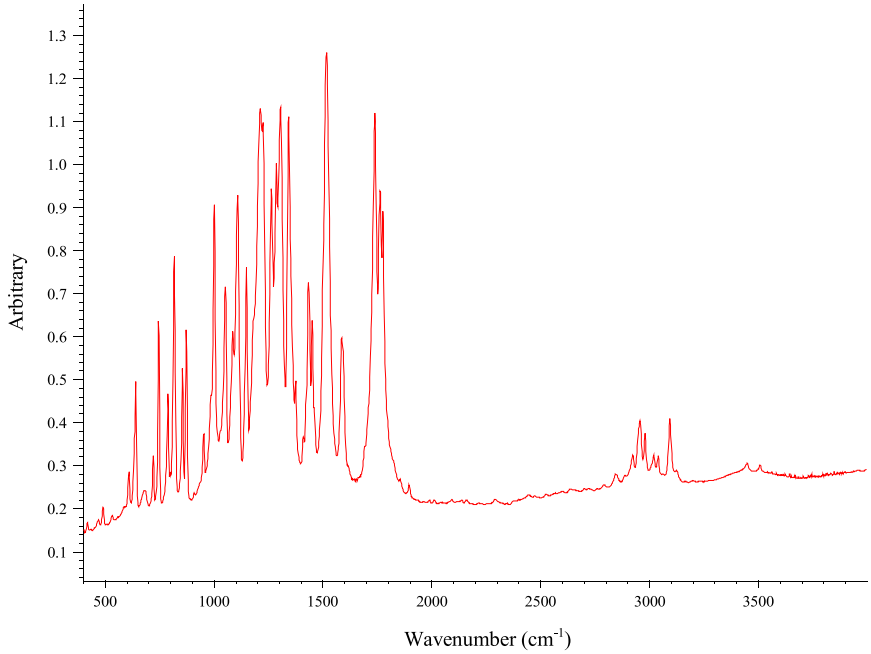

Fig. 4. The infrared spectrum of (I).

Table 1
Summary of the various vibrational modes observed in (I). Format: vibration(atoms or group) – minimum descriptive elements (PED%) γ = out of plane deformation, β = in-plane deformation, τ = torsion, ν = stretch, s = symmetric, as = asymmetric.

IR	Raman	Calcd	%PEDs
3096	3099	3145	ν(CH) (94)
3042	3047	3136	ν(CH) (89)
3021	3024	3108	ν(CH) (91)
3126		3092	$\nu_{as}(CH_3)$ (97)
3096	3100	3086	$\nu_{as}(CH_3)$ (81) $\nu(CH_3)$ (19)
3064		3059	$\nu_{as}(CH_2)$ (90) $\nu(CH_2)$ (10)
3042	3046	3054	$\nu_{as}(CH_3)$ (99)
3022	3025	3049	$\nu_{as}(CH_3)$ (99)
2981	2985	2985	$\nu_{as}(CH_2)$ (88)
	2963	2985	$\nu(CH_2)$ (84)
2951	2953	2966	$\nu(CH_3)$ (97)
2925	2929	2962	$\nu_{as}(CH_3)$ (19) $\nu(CH_3)$ (80)
	2897	2929	$\nu(CH_2)$ (95)
	2856		
	2847		
	2795		
1775			
1761	1761	1660	ν(OC) (85)
1738	1734	1626	ν(OC) (85)
	1642		
1617	1619		
1595	1595	1577	ν(Ph) (62)
1587	1585	1573	ν(Ph) (57) ν(Ph) (11)
	1534		
	1495	1482	ν(PhC–O) (12) β(Ph–H) (37) ν(Ph) (20)
	1466	1465	$\gamma(CH_2)$ (61) τ(HCOC) Ph–O (21)
1460	1460	1465	$\gamma(CH_3)$ (13) $\gamma(CH_3)$ (64) τ(HCOH) ester (22)
	1455	1457	$\gamma(CH_2)$ (58) $\gamma(CH_2)$ (13) τ(HCOH) ester (25)
1451	1451	1456	$\gamma(CH_2)$ (10) $\gamma(CH_3)$ (13) $\gamma(CH_2)$ (48)
1434	1438	1454	$\gamma(CH_3)$ (71) τ(HCOH) ester (21)
		1451	$\gamma(CH_3)$ (67) $\gamma(CH_2)$ (10)
	1425	1425	$\beta(CH_3)$ (80)
		1422	$\gamma(CH_3)$ (64)
1410		1419	ν(Ph) (33)
1375	1375	1368	τ(HCOC) Ph–O (56)
1351			
1516	1510	1358	$\nu_{as}(NO_2)$ (78)
		1345	ν(Ph) (15) τ(HCOC) Ph–O (54)
	1320	1330	ν(Ph) (17)
1305	1302		
1286	1286	1271	β(Ph–H) (50)
	1276	1259	ν(CO) ester (14) β(Ph–H) (53)
1263	1263	1239	ν(PhC–O) (29) ν(Ph) (16) β(Ph–H) (10)
1341	1342	1213	$\nu_s(NO_2)$ (67) $\beta(NO_2)$ (10)
1227	1229	1207	ν(CO) – ester C, methoxy O (26) β(Ph–H) (14)
1211		1203	$\gamma(CH_2)$ (68) τ(HCOH) Ph–O (10)
	1189	1181	ν(CO) – phenyl O (30) β(Ph–H) (17) Bing (Ph) (16)
1179	1180	1170	ν(CO) – ester C, methoxy O (53) τ(HCOC) Ph–O (10)
		1151	$\gamma(CH_2)$ (17) τ(HCOC) Ph–O (13) τ (HCOC) Ph–O (49)
		1149	$\gamma(CH_3)$ (10) $\gamma(CH_3)$ (16) τ (HCOH) ester (66)
1148	1149	1133	ν(Ph) (13) β(Ph–H) (42)
1107	1109	1116	$\gamma(CH_2)$ (19) τ (HCOH) ester (66)
		1114	$\gamma(CH_3)$ (28) τ (HCOH) ester (49)
1085	1085	1070	ν(Ph) (10) ν(CN) (17) β(Ph–H) (23)
1050	1052	1018	ν(CO) O attached to Ph, non Ph C (51)
1028	1029	1014	τ(HCOC) Ph–O (18) γ(C–C(=O)–O) (11)
		1002	$\gamma(CH_2)$ (18) τ(HCOH) Ph–O (43) γ(C–C(=O)–O) (15)
984	986	984	ν(CO) O attached to Ph, non Ph C (41)
951	953	960	γ(Ar–C[5,6]H) (out of sync) (78)
999	1001	947	ν(CO) ester-methylC (72)
		929	ν(CO) ester-methylC (69)
906	908	920	γ(Ar–C[2]H) lone H wag (81)
872	873	877	ν(CN) (12) ν(CO) – phenyl O (10) ν(CO) O attached to Ph, non Ph C (16)
854	858		$\beta(NO_2)$
719	719	856	ν(COC) – ester C, methoxy O, methyl C, simultaneous stretch (40) β (Ph) (12)
816	816	815	γ(Ar–C[5,6]H) – (in sync) (79)
797	799	782	ν(CO) – ester C, methoxy O (56)
787	788	766	ν(COC) – ester C, methoxy O, methyl C, simultaneous stretch (15) $\beta(NO_2)$ (25)
		740	ν(C–O) – Ph–C, Ph–O (11) Ph ring breath (12) $\beta(NO_2)$ (22)
	711	708	γ(Ph) (58)
745	746	696	$\gamma(NO_2)$ (75)
678	683	675	β(OCO) carbonyl C=O, methoxy O (25)

Table 1 (*continued*)

IR	Raman	Calcd	%PEDs
639	640	662	β(COC) (ester) (11) γ(CCO) – ester C, methoxy O (20)
633	634	631	β(Ph) – ring breath (22) $\beta(NO_2)$ (17)
607	608	603	β(Ph) (41)
583	587	581	τ(HCOC) – methylene C, Ph–O (19) γ(CCO) – methylene C, ester C, carbonyl O
	573	569	γ(CCO) – methylene C, ester C, carbonyl O (11) γ(CCO) – methylene C, ester C, carbonyl O
531	531	554	β(Ph) (10) γ(Ph) (10) γ(Ph) (32)
488	488	530	β(Ph) (54)
466	468	480	γ(CCO) – methoxy O, ester C (10) β(COC) – methoxy O (14) γ(Ph) (21)
416	418	462	γ(Ph) (39)
	373	428	β(CCO) – ester C, methoxy O (33) γ(Ph) (12)
	362	410	ν(CN) (11) β(Ph) (38)
	341	354	ν(CN) (10) β(CCO) – methoxy O, ester C, methylene C (13) γ (Ph) (13)
	312	330	γ(Ph) (53)
	286	302	β(COC) – methoxy O (27) β(COC) – methoxy O (27)
	257	294	β(COC) – methoxy O (66)
	242	265	β(COC) – Ph–O (36)
	216	226	β(COC) – methoxy O (21) β(CCO) – ester C, methylene C, Ph–O (12)
	204	209	$\beta(NO_2)$ (45)
	185	201	β(OCC) – Ph–O, Ph–C (46)
	168	177	τ(CCOC) – ester C, methoxy O (38) τ(CCOC) – ester C, methoxy O (18)
	144	166	$\beta(NO_2)$ (26) τ(CCOC) – ester C, methoxy O (17)
	111	157	β(CCO) – ester C, methoxy O (16) γ(Ph) (34)
		136	τ(CCOC) – ester C, methoxy O (21) γ(Ph) (11)
		124	τ(OCCO) – methylene C, ester C (42) γ(Ph) (14)
		106	τ(HCOC) methyl C, methoxy O (65) τ(HCOC) methylene C, Ph–O (15)
		100	τ(HCOC) – methyl C, methoxy O (13) τ(HCOC) methyl C, methoxy O (69)
		94	τ(CCOC) – Ph–C, Ph–C, Ph–O, methylene C (70)
		61	β(CCO) ester C, methylene C, Ph–O (23) β(COC) – Ph–C, Ph–O, methylene C (37)
		54	$\gamma(NO_2)$ (70)
		39	β(COC) – Ph–C, Ph–O, methylene C (10) $\gamma(NO_2)$ (13) τ(OCCO) – methylene C, ester C (52)
		38	τ(CCOC) – ester C, ester O (10) τ(OCCO) – methyleneC, esterC (52)
		25	τ(OCCO) – methylene C, ester C (70)
		23	τ(OCCO) – methylene C, esterC (54)

spectrum displays the three bands at 3099, 3047 and 3024 cm^{-1}. The methyl and methylene units both have asymmetric and symmetric stretches which are assigned as follows; (Raman followed by infrared) $\nu_{as}CH_3$ 2984 and 2982, $\nu_{as}CH_2$ 2962 and 2960, ν_sCH_3 2951 and 2953, ν_sCH_2 2928 and 2925 cm^{-1}.

The methyl group associated with the ester single bonded oxygen gives rise to symmetric and asymmetric deformations, the latter being linearly correlated with the symmetric deformation [13]. The computational calculations predicted the symmetric deformations to be present at 1422 and 1425 cm^{-1} whilst four asymmetric deformation modes were present at 1454, 1457, and two at 1465 cm^{-1}, which is expected for methyl groups attached to an oxygen atom with little symmetry [14]. The asymmetric deformation of the CH_3 group was assigned experimentally at 1460 cm^{-1} and its asymmetric deformation as a shoulder at 1434 cm^{-1} in the infrared spectrum. The symmetric deformation was assigned at 1437 cm^{-1} in the Raman spectrum and the asymmetric deformation was not present. The rocking mode of the methyl group on the ester is often seen as a shoulder on the C(=O)–O stretch [15] and this is the case with the title compound. The shoulder is observed at 1182 cm^{-1} in the infrared spectrum, and is absent from the Raman spectrum. The two individual methyl group rocking modes were observed in the predicted spectrum at 1149 and 1150 cm^{-1}.

The methylene deformation or scissoring mode was assigned in the infrared and Raman spectrum at 1451 cm^{-1}. This mode was predicted computationally at 1456 and 1451 cm^{-1}. The associated methylene 'wagging' mode was assigned experimentally at 1375 cm^{-1} in both infrared and Raman spectrums and was predicted computationally at 1368 and 1345 cm^{-1}. The methylene 'twist' when bonded to an ether oxygen is typically reported to be in the region of 1270 ± 40 cm^{-1} [15]. In the calculated spectrum of (I) the methylene twists were predicted much lower, at 1203 cm^{-1} for one arm. In the other arm, the twists were coupled strongly to other vibrations, namely the C–O ester stretch and the C–O ether stretch. The twist was coupled in computationally derived vibrations between 1271 and 1203 cm^{-1}, with the exception of the symmetric nitro stretch.

There are a number of modes in the region between 1300–950 cm^{-1} which are attributed to Ar–X and Ar–H in-plane deformations, however these are often coupled with aromatic ring stretching and bending modes [16]. Two significant benzene C–H in-plane deformation modes were, according to potential energy distribution analysis, not coupled to ν(Ph) modes, and one benzene C–H in-plane deformation mode was weakly coupled to a ν(Ph) mode. These absorbencies were observed in the calculated spectrum at 1271, 1259, and 1133 cm^{-1}. All three of these modes were assigned in the Raman spectrum, to bands at 1286, 1276, and 1149 cm^{-1}. One of the modes did not appear to be infrared active; these were assigned to 1286 and 1148 cm^{-1}respectively. 1,2,4-Trisubstituted benzenes show absorbances in the 1125–1090 cm^{-1} range and also absorb weakly in the 1000–960 cm^{-1} range [17].

The out of plane of aromatic C–H deformation modes, of which 1,2,4 tri-substituted benzenes have three [15], were observed in the predicted spectrum as follows: two adjacent hydrogen atoms, out of sync., 960 cm^{-1}, in sync., 815 cm^{-1}. The lone hydrogen located in the '5' position on the benzene ring was observed at 920 cm^{-1}. These theoretical values agreed well with those assigned in the experimental spectra, in which the two adjacent hydrogen atoms were observed at 953 and 816 cm^{-1} respectively in the Raman spectrum and 951 and 816 cm^{-1} in the infrared spectrum. The lone hydrogen 'wag' was assigned at 908 and 906 cm^{-1} in the Raman and infrared spectra respectively.

3.2. Ester vibrations

The characterisation of carbonyl group vibrations was simplified due to the fingerprint region being absent of commonly found vibrational modes, and the strong intensity of the carbonyl mode in

infrared [18]. Esters are found at the higher frequency range of carbonyl groups due to the electronegativity of the proximal oxygen attached to the carbonyl carbon [19] and also due to contributions from the mesomeric effect [13]. The C1 symmetry of the molecule results in one vibrational mode for each of the two groups with a wavenumber difference of 34 cm^{-1}, similar to that observed experimentally. The two separate modes were distinct in the experimental spectra, visible at 1761 and 1734 cm^{-1} with Raman, and at 1762 and 1738 cm^{-1} in the infrared spectrum. Examination of the X-ray structure reveals that the carbonyl groups are located in substantially differing chemical environments, which is likely to account for the *ca.* 100 cm^{-1} differences between the predicted and experimental models.

The oxygen-methyl carbon stretch in esters usually appears in the region of 980 ± 80 cm^{-1} [15]. This mode was physically observed at 999 cm^{-1} in the infrared spectrum and 1001 cm^{-1} in the Raman spectrum, whilst in the predicted spectrum two bands attributable to each of the individual arms at 947 and 921 cm^{-1} were observed.

The in plane deformations of the carbonyl group appear in the wide region of 715 ± 115 cm^{-1} whilst the out of plane deformation appear from 635 ± 130 cm^{-1} [15]. The in plane deformation as calculated by PED was present in both modes at 856 and 766 cm^{-1}. The mode at 856 cm^{-1} however had a much stronger contribution despite lying outside the range given by the reference. Experimentally, this mode was assigned to the bands at 719 cm^{-1} in both infrared and Raman. The out of plane deformation was observed in the calculated spectrum at 675 cm^{-1} and assigned to the bands at 683 and 678 cm^{-1} in the Raman and infrared spectra respectively.

3.3. Phenolic vibrations

The presence of the oxygen atoms located in the *meta* and *para* positions of the aryl unit gives rise to band associated with aryl and alkyl C–O stretching vibrations. Aryl–alkyl ethers have strong bands in the region 1350–1240 cm^{-1} which is attributed to the aromatic carbon–oxygen stretch, and 1050–1010 cm^{-1} attributed to the alkyl carbon–oxygen stretch [15]. The higher frequency of the aromatic carbon–oxygen is attributed to the resonance effect which gives the bond some partial double bond character increasing its force constant [20]. We suspect that this character is also responsible for the substantially differing frequencies attributed to carbon oxygen stretches at the *para* and *meta* positions. This mode was assigned for both infrared and Raman spectra at 1263 cm^{-1} in the *para* position whilst the *meta* mode was only present in the Raman spectrum at 1189 cm^{-1}. In the predicted spectrum this mode was assigned at 1239 cm^{-1} for the oxygen *para* to the nitro group, and 1181 cm^{-1} for the oxygen *meta* to the nitro group. The alkyl-O stretches were observed at 1050 cm^{-1} in the infrared spectrum and 1052 cm^{-1} in the Raman spectrum for the *para* position and 984 and 986 cm^{-1} for the *meta* position. In the predicted spectrum the modes were observed for the *para* position at 1018 cm^{-1} and *meta* position 984 cm^{-1}.

3.4. Nitro vibrations

The asymmetric stretch of the nitro group was observed in the infrared spectra as a very strong mode located at 1516 cm^{-1} which agreed well with the observation that nitro groups *para* to an electron donating group are located toward the lower frequency range typical of nitro groups [21]. We note that despite both the twisting of the nitro-benzene torsion angle and the π–π stacking effect (described below), the frequency of the vibrational mode does not differ with respect to that usually observed. The Raman spectrum had a very weak signal at 1510 cm^{-1} which we attributed to the same stretch owing to its proximity to its peak in the IR spectrum. The symmetric stretch was observed as a strong peak in both the infrared and Raman spectra at 1341 and 1342 cm^{-1} respectively, again in accordance with the previous observation. Interestingly the computationally predicted vibrational modes occurred at a significantly lower wavenumber for both symmetric and asymmetric modes of vibration, calculated at 1358 and 1213 cm^{-1} respectively. Inspection of other vibrational analysis articles [22,23] which examined molecules containing nitro groups indicated that our calculation was anomalous in its substantial deviation from experimental observations.

The Ar C–N stretch was assigned to 1085 cm^{-1} in both infrared and Raman, whilst it was calculated at 1070 cm^{-1}. Nitro groups have a characteristic absorption in the 850 cm^{-1} region which was originally attributed to a C–N vibration [24] however, is now often attributed to the NO_2 scissor vibration. [25] The scissor mode was observed in (I) at 858 and 854 cm^{-1} in the Raman and the infrared spectra respectively. In the predicted spectrum this mode is coupled strongly to ring vibrations and actually appears twice coupled with differing ring vibrations at 766 and 740 cm^{-1}. The 'wagging' and 'rocking' modes are seen in benzene rings with an electron donating group in the *meta* or *para* position at 760 ± 30 and 540 ± 30 cm^{-1} [15]. The wag was assigned at 745 cm^{-1} in the infrared and 746 cm^{-1} in the Raman spectrum. The rocking mode was assigned at 531 cm^{-1} in Raman and 530 cm^{-1} in the infrared spectrum.

3.5. Aromatic carbon vibrations

In benzene there are two ring carbon–carbon vibrations that occur at 1588 cm^{-1} and 1486 cm^{-1} respectfully. These modes are doubly degenerate in benzene systems that possess a threefold plane of symmetry and are split in systems lacking this property [13]. In the title compound the two higher frequency modes are assigned at 1595 cm^{-1} in both infrared and Raman spectra, and at 1585 and 1587 cm^{-1} in infrared and Raman respectively. These two modes were calculated at 1577 cm^{-1} and 1573 cm^{-1}. The respective bands for the lower carbon–carbon vibration is seen as a very weak mode in the Raman spectrum located at 1495 cm^{-1} and is likely lost under the very intense NO_2 mode in the infrared spectrum. This mode was computationally predicted at 1482 cm^{-1}. The second low frequency mode was assigned to 1410 cm^{-1} in the infrared and was absent in the Raman spectrum. This mode was predicted at 1419 cm^{-1} in the computational spectrum. The fifth aromatic carbon–carbon stretch which in 1,2,4-trisubstituted rings substituted with two 'light' and one 'heavy' substituent is usually observed in the 1295 ± 35 region [15]. This mode was observed in the calculated spectrum at 1330 cm^{-1} and assigned in the Raman at 1319 cm^{-1} and was absent in the infrared spectrum.

4. Geometries

The single crystal X-ray structure determination for (I) revealed that the compound crystallised as discrete molecules in the non-centrosymmetric, achiral space group $Pca2_1$. An image of the X-ray structure in comparison to the computationally derived structure is shown in Fig. 5. In the solid state the nitro group of the molecule, is twisted with respect to the plane of the benzene ring with the torsion angle C3–C4–N4–O42 = −11.9(4)°. This twist results in co-planarity with the benzene ring of an adjacent molecule in the crystal, facilitating a π–π stacking interaction which is detailed in Fig. 6. This contrasts to the planarity observed across the nitro group and aromatic ring in the predicted model.

Again in the solid state the 2-methoxy-2-oxoethanolate (2m2o) group in the *meta* position, with respect to the nitro group, is essentially co-planar with the benzene ring with the torsion angles

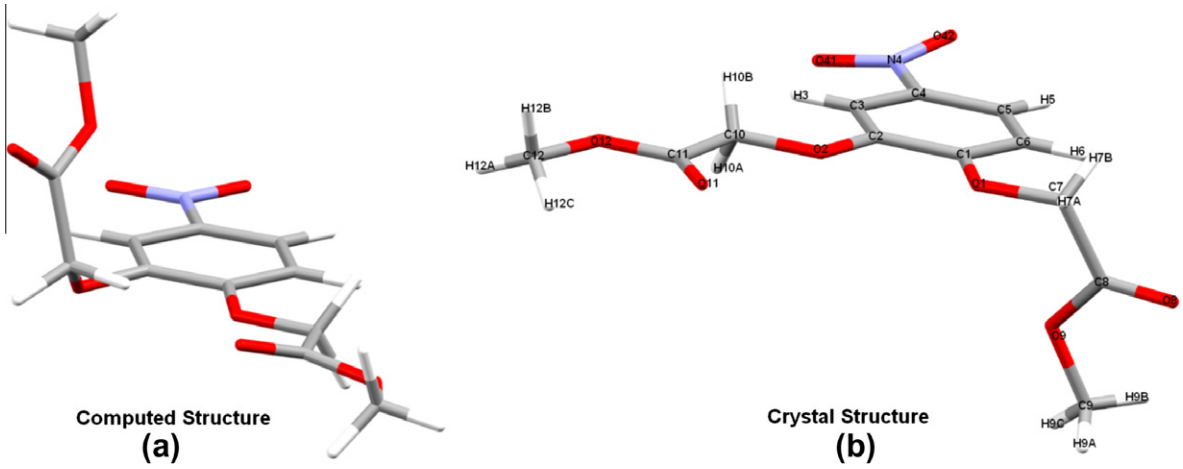

Fig. 5. (a) The predicted minimum energy geometry of (I). (b) The molecular structure of (I) as revealed by single crystal X-ray diffraction.

C3–C2–O2–C10 O2–C10–C11–O11 and O11–C11–O12–C12 being −0.6(4)°, 1.8(4)°, 0.9(5)° respectively. In contrast, the 2m2o group in the *para* position lies approximately perpendicular to the benzene ring (the C1–O1–C7–C8 torsion angle being −78.2(3)°).

The carbonyl oxygen (O8) located on the *para* 2m2o group possesses short-range interactions along the screw axis to two hydrogen atoms (H6 and H7B) with distances 2.718 and 2.380 Å for O8···H6 and O8···H7B respectively (Fig. 6). The carbonyl oxygen located on the *meta* group (O11) possesses only one short range interaction with H7A with symmetry operation $x - 1/2, 2 - y, z$. Each carbonyl group exists in substantially different chemical environments.

It can be postulated that the crystal growth along the crystallographic 'c' axis was facilitated by the aforementioned π···π interaction between the nitro group and an adjacent aromatic ring, the *para* carbonyl···H interactions, a C–H10A···π interaction and the potential overlapping of adjacent benzene π orbitals. These interactions, along with the absence of strong interactions repeating along the 'a' or 'b' axis, explains why (I) crystallises easily as long thin needles.

Computational analysis, using differences in single point potential energies of the X-ray and theoretical gas phase geometry optimised structures can approximate the crystal packing forces [26] required to maintain the molecule in its solid state conformation. Our initial analysis using this simplistic approach suggested that the compound was indeed stabilized by substantial inter-molecular forces which when calculated at the B3LYP 6-31++G level afforded a value of approximately 630 kJ/mol.

The magnitude of this crystal packing force raised a number of questions relating to both the accuracy of the computationally predicted structure as well as the magnitude of the individual short-range interactions located in the crystal structure. On closer inspection, the differences in bond lengths between the crystal structure and the computationally optimised structure differ by a small, but not insignificant amount (see Table 2). It is likely that the bond lengths in the crystal structure which differ from the predicted bond lengths could potentially have a large impact on the single point energy calculation. To address this, we adjusted the bond lengths of the geometry derived from the crystal structure to the values in the predicted structure while maintaining the bond

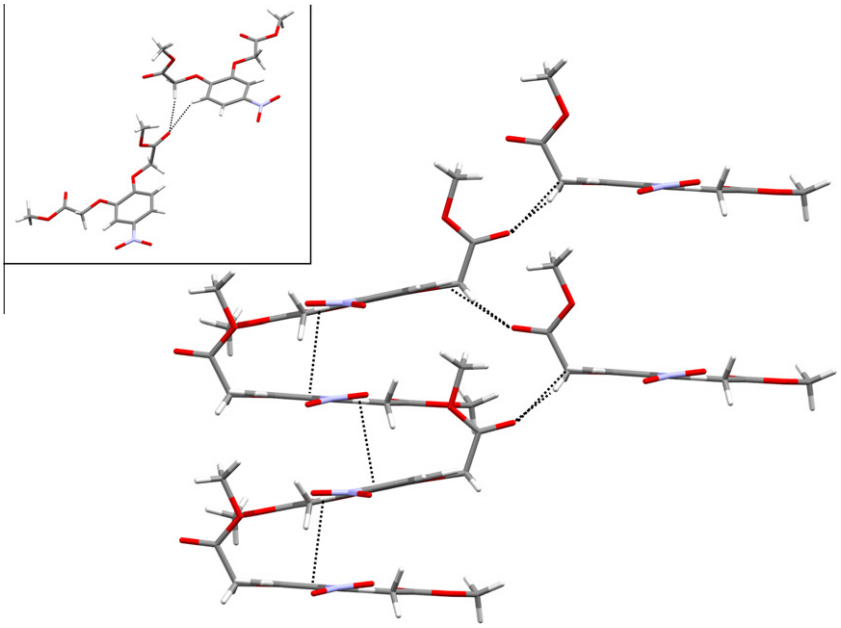

Fig. 6. The inter-molecular interactions along the crystallographic C axis. Inset: A view illustrating the O ··· H interactions.

Table 2
Summary of short contacts in the molecule.

Short contacts	Distance (Å)
O42 H5	2.53
O8–H7	2.38
O8–H6	2.72
O1–H12	2.67
O1–H10	2.57

Table 3
Total bond lengths of the various parts of the molecule.

	Total distance (Å)[a]	Total distance (Å)[b]
Benzene ring	8.335	8.401
Para arm	7.080	7.188
Meta arm	7.075	7.212
Total	22.490	22.801 (~1.4% difference)

[a] Crystal structure.
[b] Predicted structure.

angles and torsions, thus normalising the bond lengths. This resulted in a reduction of the difference in the single energy point calculations to a more realistic value of 240 kJ/mol (see Table 3).

We also calculated interaction energies of three dimer assemblies of (I) (Fig. 7) as they appear in the crystal structure. This revealed that all three interactions result in attractive forces (Table 4), however they were quite weak. We attributed this observation to a combination of basis set incompleteness for interaction energies [27] and the non-optimised geometries of the initial structures. Despite these shortcomings, the computational calculations predicted favourable interactions that may have accounted for the variations observed between the vibrational modes of experiment and theory.

Table 4
Interactions energies of selected dimer assemblies using the X-ray crystal structure geometries.

Crystal dimer assembly	Interaction energy (kJ/mol)
1	−37.4
2	−13.6
3	−7.0

5. Conclusion

This study reports both the solid state vibrational and X-ray structural analysis of a derivative of phenylenedioxydiacetic acid and compares these data to the molecules computationally predicted properties. X-ray analysis revealed the presence of numerous short-range inter-molecular forces. The theoretical method utilised, which does not take these interactions into consideration, predicted the bulk of the vibrational modes for the title compound. Two notable exceptions, however, were the nitro group symmetric and asymmetric stretches and the carbonyl symmetric stretches. This may be attributable to the observation that both of these groups are engaged in significant inter-molecular bonding as revealed by X-ray analysis and favourable interaction energy calculations. The application of potential energy distribution analysis allowed the assignment of the various vibrational modes, including the mixed modes, unambiguously.

We have revealed that the optimised geometry, as predicted computationally, deviated quite considerably from the geometry shown in the crystal structure. Subsequent analysis of the X-ray

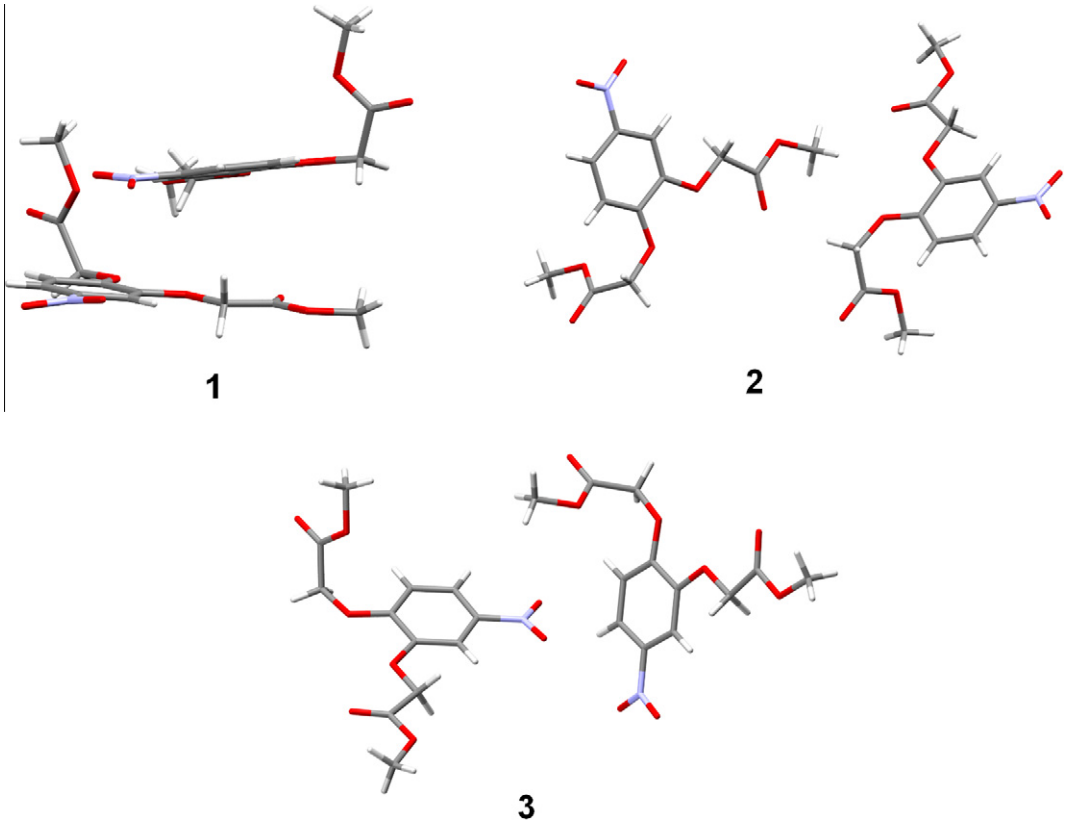

Fig. 7. The geometries of the dimer systems for the three interaction energy calculations.

structure demonstrated significant numbers of inter-molecular crystal packing forces in the solid state. These forces were estimated by calculating the two energies of the bond length normalised X-ray and computationally derived minimum energy geometries. The magnitude of this force was approximately 240 kJ/mol.

Acknowledgement

The authors thank the Australian Government for an Australian Postgraduate Award (BVC).

References

[1] L.F. Rao, G.R. Choppin, Inorg. Chem. 29 (1990) 3589.
[2] X. Li, Y.-Q. Li, X.-J. Zheng, H.-L. Sun, Inorg. Chem. Commun. 11 (2008) 779.
[3] M.B. Gholivand, A.A. Romiani, Electroanalysis 18 (2006) 730.
[4] K. Suzuki, T. Hattori, K. Yamasaki, J. Inorg. Nucl. Chem. 30 (1968) 161.
[5] teXsan, Single Crystal Structure Analysis Software. Version 1.8, Molecular Structure Corporation, Woodlands, Texas, 1997.
[6] CrysAlis, CCD Version 1.171.32.13, Oxford Diffraction Ltd., 2007.
[7] G.M. Sheldrick, Acta Crystallogr. A64 (2008) 112.
[8] L.J. Farrugia, J. Appl. Crystallogr. 30 (1997) 565.
[9] A.L. Spek, J. Appl. Crystallogr. 36 (2003) 7.
[10] M.J. Frisch, G.W. Trucks, H.B. Schlegel, G.E. Scuseria, M.A. Robb, J.R. Cheeseman, J.A. Montgomery, T.V. Jr., K.N. Kudin, J.C. Burant, J.M. Millam, S.S. Iyengar, J. Tomasi, V. Barone, B. Mennucci, M. Cossi, G. Scalmani, N. Rega, G.A. Petersson, H. Nakatsuji, M. Hada, M. Ehara, K. Toyota, R. Fukuda, J. Hasegawa, M. Ishida, T. Nakajima, Y. Honda, O. Kitao, H. Nakai, M. Klene, X. Li, J.E. Knox, H.P. Hratchian, J.B. Cross, V. Bakken, C. Adamo, J. Jaramillo, R. Gomperts, R.E. Stratmann, O. Yazyev, A.J. Austin, R. Cammi, C. Pomelli, J.W. Ochterski, P.Y. Ayala, K. Morokuma, G.A. Voth, P. Salvador, J.J. Dannenberg, V.G. Zakrzewski, S. Dapprich, A.D. Daniels, M.C. Strain, O. Farkas, D.K. Malick, A.D. Rabuck, K. Raghavachari, J.B. Foresman, J.V. Ortiz, Q. Cui, A.G. Baboul, S. Clifford, J. Cioslowski, B.B. Stefanov, G. Liu, A. Liashenko, P. Piskorz, I. Komaromi, R.L. Martin, D.J. Fox, T. Keith, M.A. Al-Laham, C.Y. Peng, A. Nanayakkara, M. Challacombe, P.M.W. Gill, B. Johnson, W. Chen, M.W. Wong, C. Gonzalez, J.A. Pople, Gaussian, Inc., Wallingford CT, 2004.
[11] K.K. Irikura, R.D. Johnson, R.N. Kacker, J. Phys. Chem. A 109 (2005) 8430.
[12] M.H. Jamróz, Warsaw, 2004.
[13] N.B. Colthup, L.H. Daly, S.E. Wiberley, Introduction to Infrared and Raman Spectroscopy, 3rd ed., Academic Press, San Diego, 1990.
[14] G. Socrates, Infrared and Raman Characteristic Group Frequencies: Tables and Charts, 3rd ed., John Wiley & Sons Ltd., West Sussex, 2004.
[15] N.P.G. Roeges, A Guide to the Complete Interpretation of Infrared Spectra of Organic Structures, John Wiley & Sons Ltd., West Sussex, 1994.
[16] J.R. Scherer, Spectrochim. Acta 21 (1965) 321.
[17] L.J. Bellamy, The Infra-red Spectra of Complex Molecules, 3rd ed., Chapman and Hall Ltd., London, 1975.
[18] R.M. Silverstein, G.C. Bassler, T.C. Morril, Spectrometric Identification of Organic Compounds, 5th ed., John Wiley and Sons Inc, Singapore, 1991.
[19] R.E. Kagarise, J. Am. Chem. Soc. 77 (1955) 1377.
[20] A.R. Katritzky, N.A. Coats, J. Chem. Soc. (1959) 2062.
[21] R.D. Kross, V.A. Fassel, J. Am. Chem. Soc. 78 (1956) 4225.
[22] V. Krishnakumara, S. Dheivamalar, J. Raman Spectrosc. 40 (2009) 411.
[23] M. Wandas, J. Lorenc, E. Kucharska, M. Mączka, J. Hanuza, J. Raman Spectrosc. 39 (2008) 832.
[24] R.R. Randle, D.H. Whiffen, J. Chem. Soc. (1952) 4153.
[25] J.H.S. Green, W. Kynaston, A.S. Lindsey, Spectrochim. Acta 17 (1961) 486.
[26] E.R.T. Tiekink, V.J. Hall, M.A. Buntine, J. Hook, Z. Kristallogr. 215 (2000) 23.
[27] G. Chalasinski, M.M. Szczesniak, Chem. Rev. 94 (1994) 1723.